High Temperature Self-Powered Sensing System for a Smart Bearing in an Aircraft Jet Engine

Bahareh Zaghari, Alex S. Weddell, *Member, IEEE,* Kamran Esmaeili,
Imran Bashir, Terry J. Harvey, Neil M. White, *Senior Member, IEEE,* Patrick Mirring, and Ling Wang

Abstract—Integrated health monitoring is beneficial but due to reliability, weight, size, wiring and other constraints, the incorporation of instrumentation onto aircraft propulsion systems is limited. Conventional wired sensing systems are not always feasible due to size, weight constraints, and issues associated with cable routing. This paper presents an integrated and self-powered wireless system for high temperature (above $125°$C) environments powered by a thermoelectric generator for bearing condition monitoring. Thermoelectric generator with internal oil cooling chamber is proposed to achieve higher energy output for small temperature gradient recorded in the jet engine in comparison with other thermoelectric generators with heat sinks. The experimental results demonstrate that, under a simulated engine environment, the thermoelectric generator can provide sufficient energy for a wireless sensing system to collect environmental data every 46 s, and transmit every 260 s, during the critical take-off phase of flight and part of cruise.

Index Terms—self-powered, condition health monitoring, wireless, aerospace.

I. INTRODUCTION

SELF-POWERED sensing systems could enhance the performance and reliability of aircraft propulsion systems. Around 50% of flight delays are due to engine problems, at a cost of US$9,000$ per hour. Furthermore, 50% of flight cancellations are due to engine problems at a cost of US$66,000$ per cancellation [1]. In the case of in-flight shut down, each engine component must be inspected individually. Hence, it is very important to monitor engine components such as bearings, and to detect an impending failure at early stage [2]. For example, an integrated wireless sensor close to a bearing could provide more accurate information about the health of the bearing. This is achieved by primarily having a direct access to the source or the component of interest and enhanced signal quality essential for early fault detection and diagnosis.

Recent investigations on bearing condition monitoring are either done by analyzing the recorded signals off-line [3, 4, 5]

B. Zaghari (Corresponding author), A. S. Weddell, and N. M. White are with the School of Electronics and Computer Science, University of Southampton, Southampton, SO17 1BJ, UK. e-mail: (bahareh.zaghari@soton.ac.uk; asw@ecs.soton.ac.uk; nmw@ecs.soton.ac.uk)

K. Esmaeili, T. J. Harvey, and L. Wang are with the National Centre for Advanced Tribology at Southampton (nCATS), University of Southampton, Southampton, SO17 1BJ, UK. I. Bashir was with the Advanced Tribology at Southampton (nCATS), University of Southampton, Southampton, SO17 1BJ, UK. e-mail: (kamran.esmaeili@soton.ac.uk; T.J.Harvey@soton.ac.uk; ling.wang@soton.ac.uk; I.Bashir@bath.ac.uk)

Patrick Mirring is from Schaeffler Aerospace, 97421 Schweinfurt ,Germany. e-mail: (mirriptr@schaeffler.com)

or on-node in room temperature [6]. On-node signal processing for initial feature extractions and fault diagnosis can be implemented on an integrated wireless sensor system. Wireless sensing systems consist of sensors, electronics (including amplifiers, Analog to Digital converters (ADCs)), power sources or storage devices, a processor and wireless transmission modules. Real-time data collection from sensors and data analytics can be used to improve performance, and reduce operational and maintenance costs. Although some transducers are suitable for high temperature applications, it is difficult to measure the process and wirelessly transmit readings in-situ owing to the lack of high temperature electronics and energy storage. Typically, data is transferred with cables to much cooler regions. In the case of a jet engine, the electronics are typically placed in the nacelle, which may range from -40°C to +55°C. Due to complex wiring connections, reliability can be poor, the sensor locations are restricted and the cost and weight of the sensing system is increased.

Smart bearings have been widely used in automotive and rail applications [7], however they have not been developed for jet engines due to the challenging operating environment. Vibration and temperature are traditionally the driving parameters for online health monitoring [8, 9]. In a recent study a signal processing technique based on undersampled vibration signals have been introduced to minimize the energy consumption and computing resource of wireless self-powered systems while retaining the monitoring and diagnosis performance [10]. As well as vibration data, load, cage and shaft speed in a jet engine have been recorded and analysed for bearing condition monitoring [11]. Suitable sensors for a jet engine were tested to find their resilience to high temperature and high shaft rotational speed (3000 rpm to 25,000 rpm), which creates a turbulent environment [12]. Apart from the environmental restrictions, wireless sensors for smart bearings must be autonomously powered, restricting the power budget for sensing and wireless data transmission. Most vibration, load, and temperature sensors do not require power for sensing, but their amplifiers do. To achieve a lighter and sustainable solution, there is a need for an energy harvester to provide energy for the sensing system.

This paper proposes an integrated self-powered smart sensing system consisting of high temperature electronics for signal amplifications, power management, processing and transmission. The system components are selected (Section II) based on their power consumption and compatibility with aerospace requirements to achieve sensing and transmission
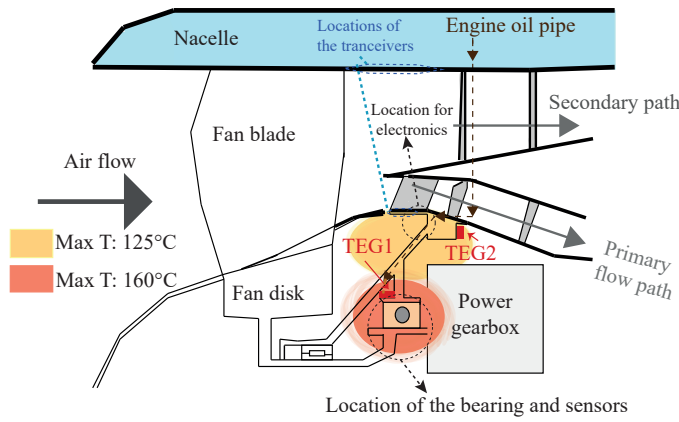
Fig. 1. Schematic of an engine part provided by Safran Aircraft Engine [17]. The smart bearing has integrated accelerometers, thermocouples, and strain gauges. Thermoelectric generators (TEGs) will be located in two places: TEG1 will be placed on the bearing outer ring and TEG2 will be under primary path and upper side of the gear box. Greater temperature variation is suitable for a thermoelectric energy harvester, hence a location close to the bearing is considered. Engine oil used for bearing lubrication will be used to cool down TEG1 and heat up TEG2. Temperature at the locations where the transceivers are attached are considered to be below 125°C.

on a typical flight profile. A system architecture has been designed (Section III), and data has been measured for energy availability from a thermoelectric energy harvester. The sensing and transmission subsystem has been designed, prototyped and characterized (Section IV), and lastly the overall power status of the system has been evaluated to model the activity of the system during a typical flight profile (Section V).

II. HIGH TEMPERATURE COMPONENT AVAILABILITY

Jet engines have several bearings at different locations. Condition monitoring of a bearing in a cooler zone (up to 125°C) is the focus of this paper, hence technologies suitable for this environment are considered. Figure 1 shows temperatures at selected locations to place the electronics and the energy harvester. The location of the bearing is close to the fan blade and in this region the temperatures do not exceed 160°C.

Vibration energy harvesters based on active materials (e.g. piezoelectric [13], magnetostrictive [14], and ferroelectric [15]) and electromechanical coupling mechanisms (e.g. electrostatic and electromagnetic [16]) have been mostly used in temperatures below 80°C. The performance of these harvesters is dependent of magnitude and the frequency of external vibration [13]. Due to elevated temperature close to the bearing, active materials have not been considered. Also magnets interfere with bearing lubrication and attract particles that need to removed by the lubrication. A thermoelectric generator, which converts heat energy to electrical energy is a popular energy harvesting mechanism in high temperature environments [18]. Thermoelectric generators (TEGs) operate on the principle that, when the connected junctions of two dissimilar materials have a temperature difference, an electrical current is generated. Typically, the best performance of the thermoelectric generators is reached when one side of the thermoelectric module is in contact with forced air convection [19]. The design presented by Zhang et al. [20]

is an example of a high temperature TEG, which is based on a nanostructured bulk material with a direct metal brazing process to increase the device operating temperature. Commercial TEGs such as Calcium/Manganese (CMO) TEG Cascade from TECTEG [21] can operate at 800°C. Ultra low power management circuits have been designed to manage the energy received from the TEGs for under 125°C [22, 23]. In these studies the design decisions are related to increasing the time that sensors can operate when the input power from the TEGs are at its minimum.

Several batteries have been developed which operate at temperatures up to 300°C under specific conditions [24]. In some aircraft, such as the Airbus A350, several SAFT Lithium-ion batteries have been packaged against high temperature, but they weigh 30 kg each [25]. The voltage level and high energy density of batteries make them suitable for wireless self-powered applications, but safety concerns about potential explosion are a significant issue for aerospace applications.

High temperature ultracapacitors (supercapacitors), or electrical double layer capacitors are also a good option for energy storage for wireless sensing modules [26, 27]. Ultracapacitors store energy through electrostatic forces, in comparison with batteries which store energy through chemical potential. Nanoramic laboratories has developed a commercially available ultracapacitor operating up to 150°C [28]. Owing to the improved safety characteristics, a lightweight ultracapacitor (FastCAP Type:EE150-35) from Nanoramic Laboratories [28] is proposed in this paper as an energy storage. This ultracapacitor contains carbon nanotubes and an electrolyte that extends the temperature range beyond other capacitors, allowing use in temperatures from -40 to +150°C. In comparison with Lithium-thionyl chloride batteries that are commonly used for high temperature systems, these ultracapacitors do not explode at shock temperatures and have lower energy density, and higher rated capacitance in comparison with other high temperature capacitors.

The commercial temperature range specification of CMOS integrated circuits is from 0°C to +85°C and -55°C to +125°C for military applications; outside these ranges is considered an extreme temperature environment [29]. Aerospace electronic systems, engine electronics, and power electronics operating temperature ranges could extend up to 500°C. However, most of these electronics are designed for high voltage and current in power plants and so are not suitable for wireless sensing systems [30]. Silicon-based CMOS devices are limited to temperatures below 500°C, due to an increase in thermal carriers in junction devices.

Wide bandgap semiconductors, such as diamond, gallium nitrides, and silicon carbide (SiC) offer great potential to fabricate high temperature electronics (>500°C) [31, 32]. New developments on 4H-SiC junction field effect transistor (JFET) ICs with two levels of interconnect have consistently demonstrated longer (>1000 hours) operating times at 500°C, which makes them more suitable for jet engine use than conventional designs. Operational testing of 4H-SiC JFET ICs at ambient temperatures up to 961°C have been reported [33]. However, plastic packages that are typically used are not

suitable for applications above 150°C. Ceramic packages for temperatures up to 500°C have been proposed [34], but are restricted to low current applications due to the resistivity of the refractory metals used as conductors [34]. Packaging technologies are the limiting factors for the industrial applications of high temperature electronics. Therefore, in order to design packaging for harsh environments, the elastic behaviour and long term stability of the micromechanical structures at elevated temperatures must be addressed [35].

Commercial products exist for high temperature data acquisition systems: the H.E.A.T. evaluation module, a high temperature signal conditioning and processor evaluation platform has been designed by Texas Instruments [36]. It is designed to withstand operating temperatures up to 210°C. The limitation of this module is the choice of amplifiers (due to limited compatibility with a few sensors) and high power consumption of its ARM7 Microcontroller, making it unsuitable for most self-powered systems. There are a few microcontrollers available for high temperature applications that consume low power, such as OMAPL137BPTPH from Texas Instruments with current consumption 20mA at 3V and an operating temperature range of -55°C to +175°C, and PC5674F from TELEDYNE e2v [37] with current consumption 3mA at 2V, and an operating temperature range of -55°C to +175°C. Electrical components should comply with DO160 specifications [12] prior to installation in the aircraft jet engine. A wireless system reduces the time and cost to install and maintain connections of large numbers of cables [38, 39]. Wireless communication of data between devices consumes power, motivating a low-power communication design. To transmit data wirelessly, communication technologies such as IEEE 802.15.4, Radio Frequency Identification (RFID), Near Field Communication (NFC), Sigfox, LoRaWAN [40], and other proprietary protocols for wireless networks have been developed. Data is received and transmitted with an RF transceiver, however, no radio chip that withstands high temperatures ($> 125°C$) is commercially available.

Passive wireless systems, Surface Acoustic Wave (SAW) resonators [41], mechanical resonator MEMS devices [42], and LC resonant devices [43] have been introduced for near field transmission. Yang [44] introduced an example of a wireless sensing device for harsh environments. The pressure sensor, a piezoresistive MEMS device, operates at 450°C. The performance of wireless transmission SiC FM module for low power devices was not evaluated in their study. Based on this review of high temperature components, the aim is to deliver a self-powered sensor system for high temperature applications (up to 125°C).

III. SYSTEM ARCHITECTURE AND DESIGN

The self-powered system is designed to provide energy for collecting data from embedded sensors (e.g. strain gauges and thermocouples) and the wireless transmission of data. Figure 2 shows the full system architecture for a high temperature self-powered sensing system and has been tested during a flight simulation (Table I). The energy evaluation has been carried out for each part of the system.
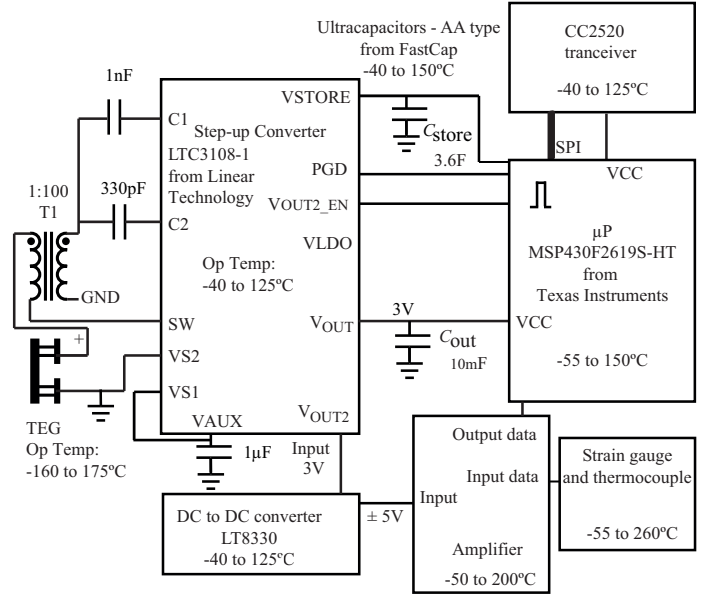

Fig. 2. The proposed wireless sensor system consists of an energy harvester, electronic interfaces, microprocessor, and wireless transmission.

TABLE I
TEMPERATURES AT TEG1 AND TEG2 LOCATIONS, AND OIL
FLOW/TEMPERATURE, FOR A SIMULATED FLIGHT.

Parameters	Phases of a flight			
	Take off (%10)	Cruise (%75)	Descent and landing (%10)	Ground idle (%5)
	TEG1 with internal cooling			
T_{oil-in}	120°C	120°C	120°C	120°C
T_{l1}	160°C	140°C	150°C	125°C
Flow rate	0.2l/min	0.2l/min	0.2l/min	0.1l/min
	TEG2 with internal heating			
T_{oil-in}	120°C	120°C	120°C	120°C
T_{l2}	120°C	115°C	120°C	100°C
Flow rate	0.2l/min	0.2l/min	0.2l/min	0.1l/min

A. Thermoelectric generator

Thermoelectric generators (TEGs) work as a heat engine operating between two heat reservoirs, as presented in Fig. 3. The efficiency of the TEG is lower than Carnot efficiency due to losses caused by the electrical, thermal, and thermoelectric properties of the thermoelectric material [45]. However, it is used in the proposed system for a non-ideal heat engine. TEGs are ideal for low power applications, and their power output can be increased by adding thermoelectric couples in series-parallel combination. In this work, Bismuth Telluride is used as a thermoelectric material [46]. In previous studies [23, 47], the characterization of thermoelectric modules for powering autonomous sensors have been done by considering the cold side with a heat sink. Here, we are showing the analysis when a cooling chamber with engine oil is considered. The efficiency of a thermoelectric device depends on electrical conductivity σ, thermal conductivity κ, and Seebeck coefficient α of the thermoelectric material. The figure of merit is defined by [18]

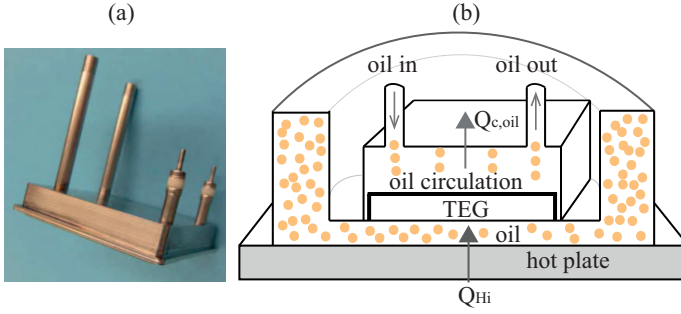$$Z = \frac{\alpha^2 \sigma}{\kappa}. \qquad (1)$$

(a) (b)

Fig. 3. (a) TEG with oil chamber. (b) Schematic of TEG1 with internal cooling oil, which is placed on a hot plate for simulating temperatures at different flight modes. The chamber with oil on the hot plate is used to distribute the temperature uniformly across the hot side of the TEG module.
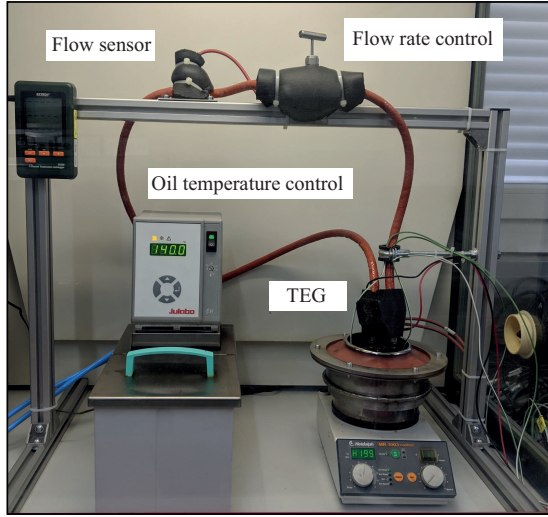

Fig. 4. Experimental set up to control the flow rate and temperature of the oil. The TEG is placed inside a chamber on a hot plate.

The electrical conductivity, thermal conductivity, and the Seebeck coefficient are functions of temperature, and change when the thermoelectric generator is encapsulated [46, 47]. Based on the energy balance at the hot and cold junctions of a thermoelectric generator [18], the heat input Q_{Hi} is balanced by Fourier heat conduction Q_{fourier}, Peltier heat Q_{peltier} and
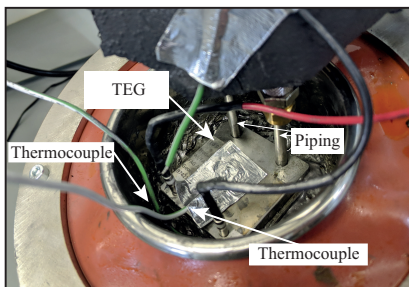

Fig. 5. TEG is placed on the hot plate. One thermocouple is placed under the TEG and the other is placed on top. Two thermocouples are placed in the piping to measure the temperature of the input and output oil. This configuration is used for simulating the engine environment, where TEG1 is located on the outer ring of the bearing.

Joule effect heat Q_{joule}, such that

$$Q_{\mathrm{Hi}} = Q_{\mathrm{fourier}} + Q_{\mathrm{peltier}} - Q_{\mathrm{joule}}, \quad (2)$$

where
$$Q_{\mathrm{fourier}} = n_{\mathrm{g}}\alpha I_{\mathrm{TEG}} T_{\mathrm{hs}}, \quad (3a)$$
$$Q_{\mathrm{peltier}} = K(T_{\mathrm{hs}} - T_{\mathrm{cs}}), \quad (3b)$$
$$Q_{\mathrm{joule}} = \frac{I_{\mathrm{TEG}}^2 R_{\mathrm{g}}}{2}, \quad (3c)$$

and n_{g} is the number of elements, α is the Seebeck coefficient, I_{TEG} is the current flow from the TEG, R_{g} is the internal electrical resistance of the TEG, and T_{hs} and T_{cs} are the hot and cold side temperatures. The thermal conductance of the encapsulated TEG K from KE technology is

$$K = 2AL^{-1}(62605.0 - 277.7T + 0.4T) \times 10^{-4} \mathrm{Wm}^{-1}\mathrm{K}. \quad (4)$$

For commercially available thermoelectric modules, A and L are approximate values for the area and the length of the P- and N-type semiconductor legs (the properties of the selected TEG from KE technology is presented in Table II). The Seebeck coefficient is

$$\alpha = \frac{V_{\mathrm{oc}}}{n_{\mathrm{g}}(T_{\mathrm{hs}} - T_{\mathrm{cs}})}, \quad (5)$$

where V_{oc} is the open circuit voltage of the TEG. The electrical current I_{TEG} flows in accordance to the applied temperature difference, which is given as

$$I_{\mathrm{TEG}} = \frac{V_{\mathrm{oc}} - V_{\mathrm{TEG}}}{R_{\mathrm{g}}}, \quad (6)$$

The electrical power, P_{measured}, harvested by the TEG is a function of its output voltage,

$$P_{\mathrm{measured}} = V_{\mathrm{TEG}} I_{\mathrm{TEG}}. \quad (7)$$

The heat absorbed by the cooling oil can be determined from the finite time thermodynamic mode [48]

$$Q_{\mathrm{C,oil}} = G c_{\mathrm{p}}(T_{\mathrm{oil-out}} - T_{\mathrm{oil-in}}), \quad (8)$$

where G is mass flow rate and c_{p} is the specific heat capacity of the cooling oil (refer to Table II), and $T_{\mathrm{oil-out}}$ and $T_{\mathrm{oil-in}}$ are the temperature of the oil coming out from the TEG and input oil temperature, respectively.

Power output can be found from this heat as

$$P_{\mathrm{calculated}} = Q_{\mathrm{Hi}} - Q_{\mathrm{C,oil}}. \quad (9)$$

B. Experimental study

Figure 1 shows the preliminary design of a jet engine with a smart bearing. The positions of the TEGs are selected based on the temperature profile of the environment. In general, a heat sink is used to cool down TEGs, however this method is not efficient for using TEGs inside a jet engine. Since there is no flow of cold air, both sides of a TEG reach a mutual temperature, leading to reduction in energy output. The selected TEGs were designed to have an internal chamber for cooling or heating. Lubricant oil (Mobil Jet Oil II) in the engine is used to cool the bearings by carrying heat away as well as collecting debris which otherwise might cause damage. A portion of this lubrication oil can be used to

cool down a TEG (TEG1 in Fig. 1), which will be installed inside the engine. The other side of the TEG is attached to a surface with a higher temperature. TEG1 is designed to give maximum power when the back is hotter than the oil circulating inside. A second TEG (TEG2 in Fig. 1) is proposed to be placed in a cooler zone, for example above the gear box in Fig 1, and hotter oil will be used to keep one side of the TEG at a higher temperature. These locations are identified based on the pathway of the oil pipes, geometry and temperature variations as well as flow rate changes during different flight phases. Circulating the oil in this way cools down the oil for TEG1 and improves the efficiency of energy harvesting. By way of experiments, TEG1 was exposed to different temperature gradients, while it was placed on a hot plate as shown in Figs. 3 and 4. In Figs. 3 and 4 the positions of the thermocouples and the piping to control the oil temperature and flow rate are shown. To simulate the engine environment the TEG is placed inside a chamber and the pipes for oil in and out are isolated from each other.

Thermal imaging techniques have been proposed as a non-invasive method for thermal characterization [47]. Since in this study the TEGs are placed inside a chamber, the thermal imaging could not be employed. Thermocouples were used to measure temperature at different positions (Fig. 5).

The voltage across different resistive loads was measured, and current and power calculated from the measured voltage and load resistance. The results at different engine operating temperatures are shown in Figs. 6 and 7. From these, the maximum power and optimum load resistance at each temperature gradient can be calculated. The voltage and current values were recorded in the steady-state mode after the load changes were applied. The optimum load varies with temperature as well as flow rate, and in Fig. 6 the peak power is found where the optimum load is close to 2 Ω. The open circuit voltage V_{OC} was measured and is shown in Fig. 6.

C. Performance of TEG1 during a simulated flight

To analyse the feasibility of using a TEG to power sensors on a smart bearing, TEG1 was tested with temperature values from a real flight program. The parameters of this test are chosen based on Table I. Table I shows the temperatures during different flight modes based on thermodynamic finite element modelling of the engine. T_{l1} and T_{l2} in Table I refer to the temperatures at the location of TEG1 and TEG2. The oil flow rates and the oil temperatures are defined by flight phases and the requirements given from the jet engine manufacturer. Oil flow rates 0.2l/min and 0.1l/min are used for the tests during take off and landing respectively.

Figure 8 shows the calculated and measured power during a flight. The 90-minute simulated flight from London to Frankfurt consists of 9 minutes for take off, 67.5 minutes for cruise, 9 minutes for descent and landing and 4.5 minutes for ground idle. The power shown in Fig. 8 is calculated by substituting Eqs. 2 and 8 into Eq. 9. The maximum loads were identified from Fig. 6. The measured power is found from the current across an optimum load resistance multiplied by the

TABLE II
PROPERTIES OF MOBIL JET OIL II AND TEGS.

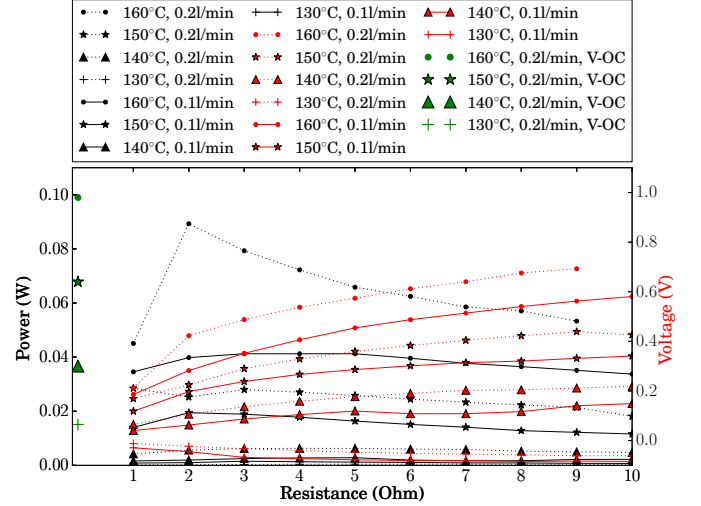| Property	Value	Units
Oil specific heat capacity	2000	$J(kgK)^{-1}$
Number of thermocouple elements	111	pairs
Dimensions of the encapsulation base	35×40	mm×mm
Module thickness (baseplate and electrode)	3	mm

Fig. 6. Measured power and voltage as a function of load resistance at different thermal gradient and oil flow rate. The temperature of the hot side and oil flow rate is defined for each point. The input oil temperature was set to 120°C.

voltage across the TEG. The measured power is less than the calculated power due to energy conversion inefficiencies and thermal losses.

The measured power output can be used to compare the proposed system with existing self-powered systems. The power generated from this study is ten times greater than the one reported in similar studies for a similar temperature difference [49]. However, exiting self-powered systems [46, 45] are designed for low temperature (under 80°C), hence the power management systems are different. Also greater temperature differences are generally considered for the thermoelectric generators making it difficult to have a like to like comparisons. During the tests shown in Fig. 8, the temperatures of the hot and cold sides of the TEG were recorded and is shown in Fig. 9. Temperature in close vicinity to the TEG1 is recorded to monitor the changes in the environment (Fig 9(c)). The voltage across the TEG1 was recorded when the load circuit was connected to the TEG1 (Fig 9(d))). The temperature of the oil $T_{\mathrm{oil-in}}$ and $T_{\mathrm{oil-out}}$, the calculated temperature difference, as well as the oil flow rate are shown in Fig. 10. These temperatures were controlled to match the requirements mentioned in Table I, however in some cases (especially between the flight phases) the temperatures differ slightly. The oil flow rate also changes with temperature and hence for the last phase of flight, the ground idle phase, the minimum flow rate of 0.1l/min has not been achieved.

IV. SENSORS AND INTERFACES

A strain gauge (Type ZFCAL-1-11) and a K-type thermocouple were selected to measure the axial and radial load and
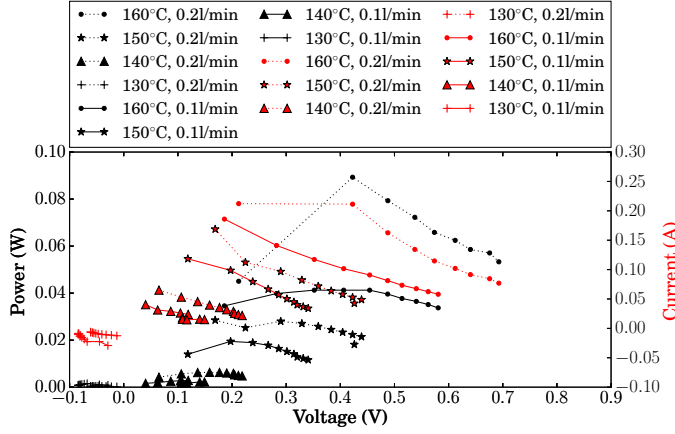
Fig. 7. Measured power and current as a function of load resistance at different thermal gradient and oil flow rates. The temperature of the hot side and oil flow rate is defined for each point. The input oil temperature was set to 120°C.
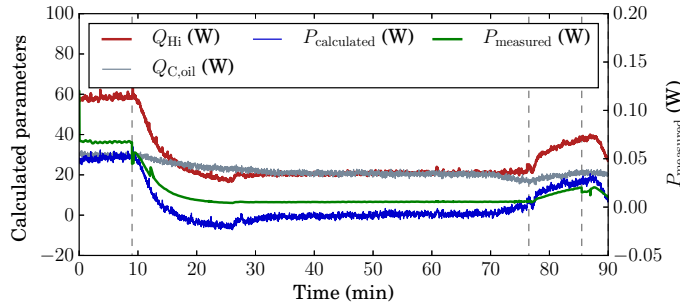

Fig. 8. Calculated power (shown in blue line) from input heat (shown by the red line) and cooling oil absorbed heat (shown in gray line) during the simulated 90 minute flight. The green line shows the measured power. The dashed lines correspond to the end of each flight phase.
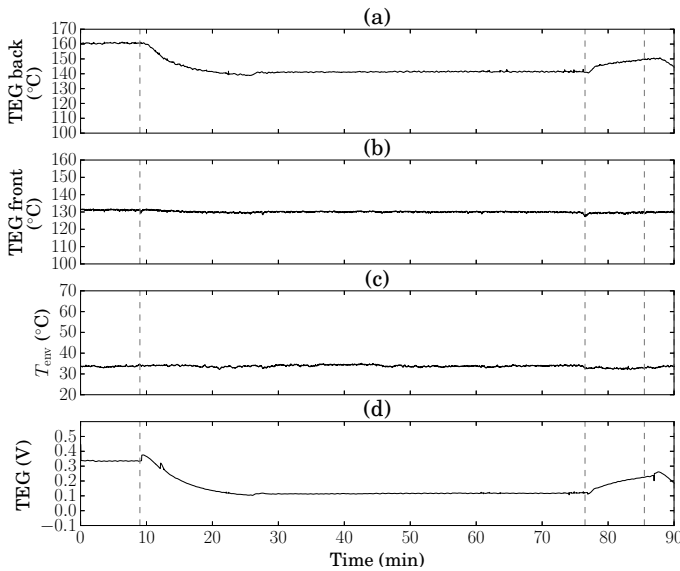

Fig. 9. (a) Temperature at the back (hot side) and (b) temperature at the front of TEG1 was recorded by the thermocouples. The temperature at the back of TEG1 is selected based on T_{11} in Table I. (c) Temperature in close vicinity to the TEG1 (approximately 4cm above TEG1). (d) Measured V_{TEG} at different phases of the flight. The dashed lines correspond to the end of each flight phase.
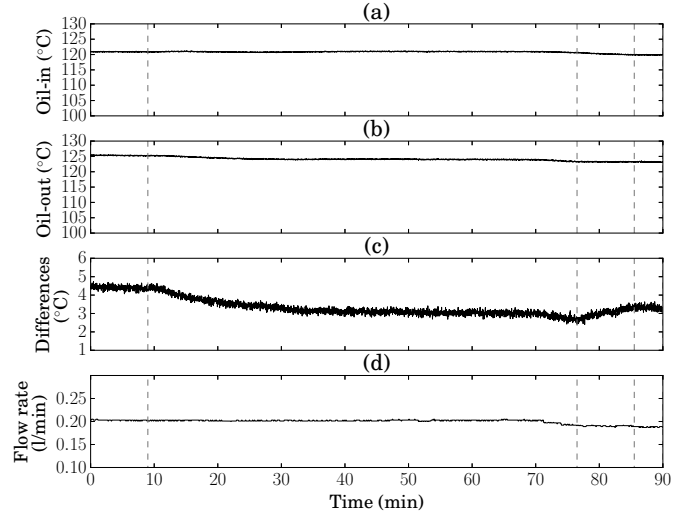

Fig. 10. (a) Temperature of oil flowing in TEG1, (b) temperature of oil flowing out TEG1, and (c) their difference at various phases of flight. (d) Oil flow rate was controlled based on the requirements in Table I. The dashed lines correspond to the end of each phase of flight.

the temperature of the bearing (refer to Fig. 11). The Gauge factor of the strain gauges at 100°C and 200°C are 1 and 2.3 respectively. $\pm 0.85[(\mu m/m)/°C]$ tolerance is considered for the strain gauges. A half bridge configuration with temperature compensation is designed. The sensors are mounted on the stationary part of the bearing (outer ring) to minimize their influence on the normal operation of the bearing. In the current set up, the sensors are connected to the processing system using cables; it is expected that, in future iterations, the wires can be robustly mounted onto the surface of the bearing housing.

A high temperature amplifier was designed using high temperature op-amps (OPA2333HT and OPA211HT) from Texas Instruments. The operating temperature range for the op-amps used to design the amplifier is -50°C to +200°C. The maximum temperature of this module restricts the operating temperature of the amplifier, with other components (capacitors and resistors) being rated at higher temperature. A Polyimide-based laminate (P26) and core material (P96) with a glass transition temperature of 260°C, was used for the printed circuit board. Calculated lifetime of a bearing is close to 90000 hours and the electronics used in the engine are specially designed and tested to have similar lifetime. In this study off the shelf components with 7000 hours lifetime have been used but for the final test demonstrator specific electronics will be made to comply with aerospace certifications.

A. Power management and energy storage

Power management is necessary since active electronics, integrated circuitry, and wireless communications all require power. Maximum Power Point Tracking (MPPT), which can be included in charge controllers are used for maximizing the power extracted from energy harvester modules. Power management ICs that can provide MPPT are not yet available for temperatures above 125°C. A boost converter (Linear
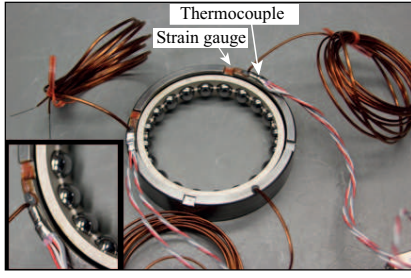
Fig. 11. Strain gauges and thermocouples mounted on a bearing.

TABLE III
MEASURED AVERAGE POWER CONSUMPTION DURING DIFFERENT MODES
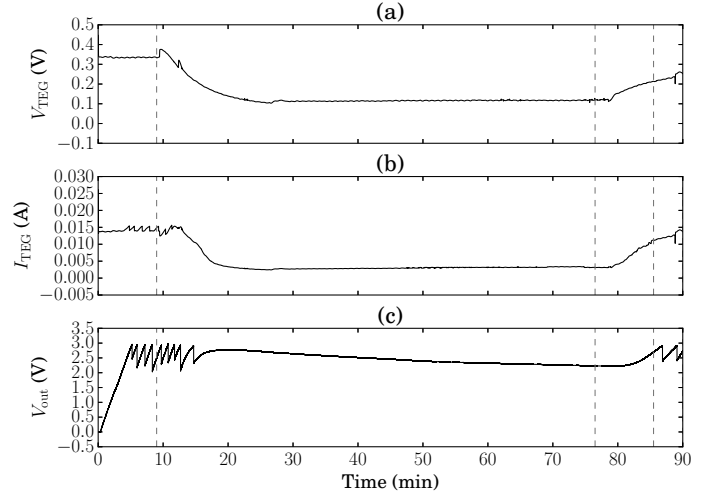AND AVERAGE DURATION OF EACH ACTIVITY.

Sleep	ADC	Transmission
Power	**Power**	**Power**
1.65 μW	0.004 W	0.09 W
Duration	**Duration**	**Duration**
Varied depend on the energy availability	0.03 sec	0.14 sec
-	**Sampling freq**	**Data size**
-	200k samples/second	230 samples

Technology LTC3108-1), which can convert the input voltage from the TEG from as low as 20 mV to 500 mV as well as managing the energy distribution between the supercapacitors and the voltage output, was selected. The proposed design (Fig. 2) has five ultracapacitors that are connected in series. Each ultracapacitor has a rated voltage of 1 V and capacitance of 33.2F. Due to their high capacitance, and the low power output of TEG, approximately 10 hours of flight would be required to fully charge the ultracapacitors. These ultracapacitors were selected based on the restrictions in using storage devices in aircraft engine.

## V. POWER CONSUMPTION ANALYSIS

A. Processing and transmission

The selected high temperature low power microcontroller unit (MCU), the MSP430F2619S-HT from Texas Instruments [36], has a 16-Bit microcontroller, 120 kB Flash, 4 kB

Fig. 12. (a) Recorded voltage and (b) current of the TEG during processing and transmission. (c) V_{out} is the voltage output of the LTC3108-1 connected to V_{CC} of the microcontroller where $C_{\text{out}} = 5\text{mF}$.

Fig. 13. (a) Recorded voltage and (b) current of the TEG during processing and transmission. (c) V_{out} is the voltage output of the LTC3108-1 connected to V_{CC} of the microcontroller where $C_{\text{out}} = 10\text{mF}$.

RAM, and a 12-bit ADC. Currently this is the only commercial MCU available with maximum operating temperature 150°C that is suitable for smart sensing. A low power radio module (CC2520 from Texas Instruments) with a 2.4 GHz IEEE 802.15.4 transceiver has also been selected, which can operate up to 125°C. One of the challenges in transmitting data wirelessly inside the jet engine is the interferences and barriers due to complex design of the engine. To avoid this during transmission, transceivers can be placed outside the outer casing of the Nacelle and close to the primary flow path as shown in Fig 1. The transceivers should be implemented using a flat antenna to prevent interferences with the flow pathways. The transceivers located in the Nacelle will be powered by the main supply available in the Nacelle. The selected locations provide a short distance for transmissions ($\leq$1m). In this study the transmit mode is set to a minimum to reduce its power consumption for short distances. The power consumption of the radio module changes based on its activity and the radio transmission power, however in comparison with other high temperature radio modules, it has the lowest power consumption in active and sleep modes.

The smart sensing system can provide enough energy for data acquisition and data transmission during take off and landing. The energy provided by TEG1 is at its highest during take off and landing due to high temperature variation. Table III shows the average power consumption measured at different stages of processing, sleep, sampling, and transmission. The average power consumption is defined for a given activity, durations, data size, and input voltages. The input voltages are stated in Fig. 2. Data transmission compared to ADC data processing has higher power consumption, but it only occurs once per several ADC processing. Figures 12 and 13 show, for a full flight, the measured voltages and current of the TEG1, as well as V_{out}, which is connected to the V_{CC} of the microprocessor.

From power consumption and its duration (t_{d}), load current
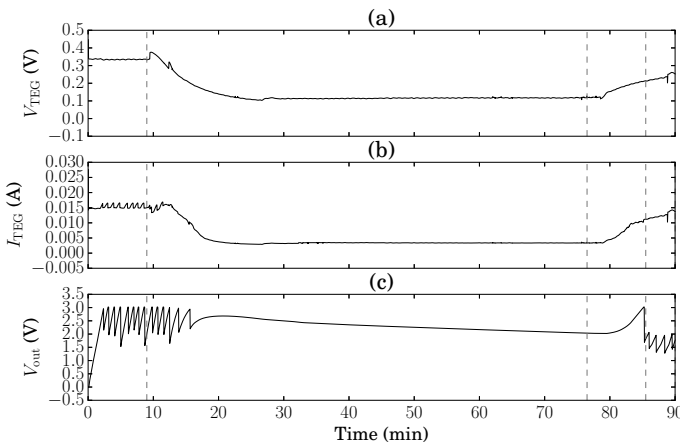
(I_{load}), and the amount of voltage drop (ΔV_{out}), the capacitance of capacitor C_{out} can be calculated as follows

$$C_{\text{out}} \geq \frac{I_{\text{load}} t_{\text{d}}}{\Delta V_{\text{out}}}. \qquad (10)$$

This calculation identifies $C_{\text{out}} = 5\text{mF}$ and $C_{\text{out}} = 10\text{mF}$ as the minimum and maximum capacitance values that achieve optimum charge time. A capacitor with $C_{\text{out}} = 5\text{mF}$ is charged within approximately 138 sec of take off (Fig. 12(c)), whereas the capacitor with $C_{\text{out}} = 10\text{mF}$ is charged after 310 sec (Fig. 13(c)). The processor is programmed to send a trigger to activate pin V_{out_2} when V_{out} on the LTC3108-1 reaches 3V, and to collect data from the thermocouple and the strain gauge's amplifier. A packet containing this data is sent wirelessly after the fourth sample.In Fig. 12(c), before reaching 20 minutes into the flight, three transmissions, each containing data from four samples, are sent approximately every 45 sec. Between samples and transmission, both the wireless module and the processor are in low power mode. This behaviour is different when a capacitor with greater capacitance is selected ($C_{\text{out}} = 10\text{mF}$). Before reaching 20 minutes into the flight, two transmissions are sent approximately every 46 sec.By selecting the minimum capacitance, the number of samples and transmissions has increased. However, using the smaller capacitor may cause the microprocessor to turn off completely when V_{CC} is less than the operating voltage of the microprocessor. Using the smaller capacitor, the voltage into the microprocessor drops to 1.5V at the end of the flight, which could lead to data loss. Further work with this system should either use the larger capacitor to avoid this data loss, or should supplement the smaller capacitor with a backup storage capacitor, with capacitance C_{store}, so that data is not lost at the end of the flight.

VI. CONCLUSION

Wireless high temperature self-power sensor technology is needed to provide in situ health monitoring in bearings. This paper highlighted the needs, opportunities, and the challenges in designing a high temperature sensing system with current available technology. Also, it discussed the feasibility of using smart sensing for engine monitoring when the electronics are designed to consume low power and by managing the energy harvesting system to provide sufficient energy for processing and transmission. The sensing system successfully operated under a controlled experiment, mimicking a real flight profile. The energy generated during take off has been enough for processing and transmission but the energy generated by TEG1 is not enough for sampling or transmission during cruise. Hence TEG2 can be used to provide more energy. Future study will be carried out when the high temperature oil from TEG1 will be used to heat up the hot side of the TEG2 and the energy availability will be analysed.

ACKNOWLEDGEMENT

REFERENCES

[1] "Air Transport Association (IATA) Safety Report," www.boeing.com/commercial/aeromagazine, accessed: 2019-07-08.
[2] Y. Zhang, H. Zuo, and F. Bai, "Classification of fault location and performance degradation of a roller bearing," *J. Meas.*, vol. 46, no. 3, pp. 1178–1189, 2013.
[3] S. S. Udmale and S. K. Singh, "Application of spectral kurtosis and improved extreme learning machine for bearing fault classification," *IEEE Trans. Instrum. Meas.*, vol. 68, no. 11, pp. 4222–4233, 2019.
[4] S. Wang, X. Chen, C. Tong, and Z. Zhao, "Matching synchrosqueezing wavelet transform and application to aeroengine vibration monitoring," *IEEE Trans. Instrum. Meas.*, vol. 66, no. 2, pp. 360–372, 2016.
[5] J. Liu, W. Wang, and F. Golnaraghi, "An enhanced diagnostic scheme for bearing condition monitoring," *IEEE Trans. Instrum. Meas.*, vol. 59, no. 2, pp. 309–321, 2009.
[6] R. Vignesh, R. Karuppiah, A. S. Ramirez, B. J. van der Zwaag, N. Meratnia, and P. Havinga, "Energy-efficient on-node signal processing for vibration monitoring," in *ISSNIP*. IEEE, 2014, pp. 1–6.
[7] S. Lu, Q. He, F. Hu, and F. Kong, "Sequential multiscale noise tuning stochastic resonance for train bearing fault diagnosis in an embedded system," *IEEE Trans. Instrum. Meas.*, vol. 63, no. 1, pp. 106–116, 2013.
[8] Y. G. Li, "Performance-analysis-based gas turbine diagnostics: A review," *Proc. Inst. Mech. Eng., Part A: J. Power and Energy*, vol. 216, no. 5, pp. 363–377, 2002.
[9] A. J. Volponi, "Gas turbine engine health management: past, present, and future trends," *J. Eng. Gas Turb. Power*, vol. 136, no. 5, p. 051201, 2014.
[10] S. Lu, P. Zhou, X. Wang, Y. Liu, F. Liu, and J. Zhao, "Condition monitoring and fault diagnosis of motor bearings using undersampled vibration signals from a wireless sensor network," *J. Sound and Vibration*, vol. 414, pp. 81–96, 2018.
[11] I. Bashir, L. Wang, T. Harvey, B. Zaghari, A. Weddell, and N. White, "Integrated smart bearings for next generation aero-engines, Part I: Development of a sensor suite for automatic bearing health monitoring." WCCM, UK, 2017.
[12] I. Bashir, B. Zaghari, T. J. Harvey, A. S. Weddell, N. M. White, and L. Wang, "Design and testing of a sensing system for aero-engine smart bearings," in *MDPI, EuroSensors2018*, vol. 2, no. 13, 2019, p. 1005.
[13] C. Trigona, B. Andò, and S. Baglio, "Performance measurement methodologies and metrics for vibration energy scavengers," *IEEE Trans. Instrum. Meas.*, vol. 66, no. 12, pp. 3327–3339, 2017.
[14] M. Zucca and L. Callegaro, "A setup for the performance characterization and traceable efficiency measurement of magnetostrictive harvesters," *IEEE Trans. Instrum. Meas.*, vol. 64, no. 6, pp. 1431–1437, 2014.
[15] Z. Luo, D. Zhu, and S. Beeby, "An electromechanical model of ferroelectret for energy harvesting," *J. Smart Mater. Struct.*, vol. 25, no. 4, p. 045010, 2016.
[16] K. Pancharoen, D. Zhu, and S. Beeby, "Temperature dependence of a magnetically levitated electromagnetic vibration energy harvester," *Sens. Actuators A, Phys*, vol. 256, pp. 1–11, 2017.
[17] "Safran," https://www.safran-group.com, accessed: 2019-06-09.
[18] D. M. Rowe, *CRC handbook of thermoelectrics*. CRC press, 1995.
[19] B. Zaghari, A. Weddell, N. White, I. Bashir, T. Harvey, and L. Wang, "Integrated smart bearings for next generation aero-engines, Part II: energy harvesting and wireless communication development." WCCM, UK, 2017.
[20] Y. Zhang, M. Cleary, X. Wang, N. Kempf, L. Schoensee, J. Yang, G. Joshi, and L. Meda, "High-temperature and high-power-density nanostructured thermoelectric generator for automotive waste heat recovery," *J. Energy Convers. Manag*, vol. 105, pp. 946–950, 2015.
[21] "TECTEG MFR. thermoelectric technology," https://www.tecteg.com/, accessed: 2019-06-09.
[22] P. C. Dias, F. J. O. M. Morais, M. B. Franca, E. C. Ferreira, A. Cabot, and J. A. S. Dias, "Autonomous multisensor system powered by a solar thermoelectric energy harvester with ultralow-power management circuit," *IEEE Trans. Instrum. Meas.*, vol. 64, no. 11, pp. 2918–2925, 2015.
[23] S. Dalola, M. Ferrari, V. Ferrari, M. Guizzetti, D. Marioli, and A. Taroni, "Characterization of thermoelectric modules for powering autonomous sensors," *IEEE Trans. Instrum. Meas.*, vol. 58, no. 1, pp. 99–107, 2008.
[24] D. Kumar, S. K. Rajouria, S. B. Kuhar, and D. Kanchan, "Progress and prospects of sodium-sulfur batteries: A review," *J. Solid State Ion.*, vol. 312, pp. 8–16, 2017.
[25] J.-M. Dilhac and V. Boitier, *Energy Autonomy of Batteryless and Wireless Embedded Systems: Aeronautical Applications*. Elsevier, 2016.

[26] R. Vellacheri, A. Al-Haddad, H. Zhao, W. Wang, C. Wang, and Y. Lei, "High performance supercapacitor for efficient energy storage under extreme environmental temperatures," *Nano Energy*, vol. 8, pp. 231–237, 2014.

[27] B. Zaghari, I. Bashir, A. S. Weddell, N. M. White, T. J. Harvey, and L. Wang, "Oil-cooled thermoelectric energy harvesting for aero-engine sensing system," in *MDPI, EuroSensors2018*, vol. 2, no. 13, 2018, p. 965.

[28] "Fastcap Systems," https://www.nanoramic.com, accessed: 2019-06-09.

[29] A. Hassan, Y. Savaria, and M. Sawan, "Electronics and packaging intended for emerging harsh environment applications: A review," *IEEE Trans. Very Large Scale Integr. (VLSI) Syst.*, 2018.

[30] B. Zaghari, A. Weddell, and N. White, "Opportunities and challenges for energy harvesting sensor systems for harsh environments." ENSsys 2017, Delft, Netherlands, 2017.

[31] W. R. Fahrner, R. Job, and M. R. Werner, "Sensors and smart electronics in harsh environment applications," *J. Microsystem Tech*, vol. 7, no. 4, pp. 138–144, 2001.

[32] D. G. Senesky, B. Jamshidi, K. B. Cheng, and A. P. Pisano, "Harsh environment silicon carbide sensors for health and performance monitoring of aerospace systems: A review," *IEEE Sensors Journal*, vol. 9, no. 11, pp. 1472–1478, 2009.

[33] P. G. Neudeck, D. J. Spry, L. Chen, N. F. Prokop, and M. J. Krasowski, "Demonstration of 4H-SiC digital integrated circuits above 800 c," *IEEE Electron Device Lett.*, vol. 38, no. 8, pp. 1082–1085, 2017.

[34] M. R. Werner and W. R. Fahrner, "Review on materials, microsensors, systems and devices for high-temperature and harsh-environment applications," *IEEE Trans. Ind. Electron*, vol. 48, no. 2, pp. 249–257, 2001.

[35] P. Hagler, P. Henson, and R. W. Johnson, "Packaging technology for electronic applications in harsh high-temperature environments," *IEEE Trans. Ind. Electron*, vol. 58, no. 7, pp. 2673–2682, 2011.

[36] "Texas Instruments," https://www.ti.com, accessed: 2019-06-09.

[37] "Teledyne e2v," https://www.teledyne-e2v.com/, accessed: 2019-06-09.

[38] W. C. Wilson and P. D. Juarez, "Emerging needs for pervasive passive wireless sensor networks on aerospace vehicles," *Procedia Computer Science*, vol. 37, pp. 101–108, 2014.

[39] M. C. Scardelletti, J. L. Jordan, G. E. Ponchak, and C. A. Zorman, "Wireless capacitive pressure sensor with directional RF chip antenna for high temperature environments," in *(WiSEE)*. IEEE, 2015, pp. 1–6.

[40] M. Rizzi, P. Ferrari, A. Flammini, and E. Sisinni, "Evaluation of the IoT LoRaWAN solution for distributed measurement applications," *IEEE Trans. Instrum. Meas.*, vol. 66, no. 12, pp. 3340–3349, 2017.

[41] G. Schimetta, F. Dollinger, G. Scholl, and R. Weigel, "Wireless pressure and temperature measurement using a SAW hybrid sensor," in *IEEE Ultrasonics Symposium, 2000*, vol. 1. IEEE, 2000, pp. 445–448.

[42] A. J. Knobloch, F. R. Ahmad, D. W. Sexton, and D. W. Vernooy, "Remote driven and read MEMS sensors for harsh environments," *J. Sensors*, vol. 13, no. 10, pp. 14 175–14 188, 2013.

[43] Y. Wang, Y. Jia, Q. Chen, and Y. Wang, "A passive wireless temperature sensor for harsh environment applications," *J. Sensors*, vol. 8, no. 12, pp. 7982–7995, 2008.

[44] J. Yang, "A harsh environment wireless pressure sensing solution utilizing high temperature electronics," *J. Sensors*, vol. 13, no. 3, pp. 2719–2734, 2013.

[45] S. Manikandan and S. C. Kaushik, "Thermodynamic studies and maximum power point tracking in thermoelectric generator thermoelectric cooler combined system," *Cryogenics*, vol. 67, pp. 52–62, 2015.

[46] M. Kambe, R. Morita, K. Omoto, Y. Koji, T. Yoshida, and K. Noishiki, "Thermoelectric power conversion system combined with LNG vaporizer," *J. Power and Energy Systems*, vol. 2, no. 6, pp. 1304–1319, 2008.

[47] F. Attivissimo, A. D. Nisio, C. G. C. Carducci, and M. Spadavecchia, "Fast thermal characterization of thermoelectric modules using infrared camera," *IEEE Trans. Instrum. Meas.*, vol. 66, no. 2, pp. 305–314, 2016.

[48] F. Meng, L. Chenand, Y. Feng, and B. Xiong, "Thermoelectric generator for industrial gas phase waste heat recovery," *Energy*, vol. 135, pp. 83–90, 2017.

[49] D. S. D, M. Kluge, T. Becker, and U. Schmid, "Wireless sensor node powered by aircraft specific thermoelectric energy harvesting," *Sens. Actuators A, Phys*, vol. 172, no. 1, pp. 240–244, 2011.

Bahareh Zaghari received M.Sc degree (Hons) in Electromechanical Engineering in 2012 from the University of Southampton, U.K. She received her PhD in Dynamic analysis of a nonlinear parametrically excited system using electromagnets from Institute of Sound and Vibration (ISVR) at the University of Southampton in 2017. Currently she is a Research Fellow at the school of Electronics and Computer Science, and she is working on the design of smart systems, such as the next generation of jet engines and smart cities.

Alex S. Weddell received the M.Eng. degree (1st class honors) and Ph.D. in electronic engineering from the University of Southampton, U.K., in 2005 and 2010. His main research focus is in the areas of energy harvesting and energy management for future Internet of Things devices. He has over 14 years experience in design and deployment of energy harvesting systems, and has published around 55 peer-reviewed papers in the area. He is currently a Lecturer in the Center for Internet of Things and Pervasive Systems at the University of Southampton, and is involved with three projects funded by EPSRC, EU Horizon 2020 and Clean Sky 2.

Kamran Esmaeili graduated from the University of Southampton in 2016 with a degree in M.Eng. Mechanical Engineering with a semester in industry. In 2016, he started his PhD research within the nCATS group at the University of Southampton. Currently, he is also a part-time researcher within the Integrated Intelligent Bearing Systems (I2BS) project, focusing on the development of bearing fault detection systems. He has a special interest in the areas of bearing tribology and bearing condition monitoring.

Imran Bashir received B.Eng (hons) in Electrical Engineering from COMSATS University, Pakistan (2008), M.Sc in Data communication from University of Sheffield, U.K. (2010) and his PhD in Acoustics Meta-materials from The Open University, UK (2014). He worked as a postdoc researcher at the University of Exeter and University of Southampton. Currently, he is working at the University of Bath, where his research is focused on Aero-acoustics Meta-materials. His research interests are Acoustics, Vibrations and condition monitoring.

Terry J. Harvey received his BSc (Hons) in Applied Chemistry at the University of Portsmouth in 1994 and PhD in the same institution in 1997. Terrys main areas of research are tribology and condition monitoring. He has over 20 years of experience in these areas producing 57 journal and conference papers. Terry is currently Senior Research Fellow working on five projects (three European Horizon 2020 projects, as well as one Innovate UK and one EPSRC projects).

Neil M. White (M01SM02) received the Ph.D. degree from the University of Southampton, Southampton, U.K., in 1988, for a thesis describing the piezoresistive effect in thick-film resistors. He was appointed as a Lecturer within the School of Electronics and Computer Science in 1990 and promoted to Senior Lecturer in 1999, Reader in 2000, and was awarded a Personal Chair in 2002. He lectures on electronic circuits, MEMS and advanced instrumentation and sensors. He has co-authored several text books and has published more than 250 scientific papers in the area of sensors and energy harvesting systems. He holds ten patents. He was the recipient of the 2009 Calendar Silver Medal, awarded by the Institute of Measurement and Control for his outstanding contribution to the art of instruments and measurement.

Patrick Mirring is the Head of Research & Development at Schaeffler Aerospace Germany. He received his Diploma degree in mechanical engineering from Baden-Wuerttemberg Cooperative State University (DHBW) in 2006. He started his career in Fundamental Research Department at Schaeffler in 2006. Since 2011 he has worked as a Development Engineer in the Advance Development of FAG Aerospace, co-ordinating multiple national and international funded R&D projects. In his current position, he is responsible for advance development, material development and design of Aerospace bearings e.g. main shaft engine bearings and swash plate bearings in helicopters.

Ling Wang is a Professor of Tribo-Sensing and Head of the national Centre for Advanced Tribology at Southampton (nCATS) in University of Southampton, UK. Her research focuses on tribology and sensing of tribological systems including developing smart bearings using artificial intelligence and machine learning techniques.